PALEOCLIMATE

Antarctic surface temperature and elevation during the Last Glacial Maximum

Christo Buizert[1]*, T. J. Fudge[2], William H. G. Roberts[3], Eric J. Steig[2], Sam Sherriff-Tadano[4], Catherine Ritz[5], Eric Lefebvre[5], Jon Edwards[1], Kenji Kawamura[6,7,8], Ikumi Oyabu[6], Hideaki Motoyama[6], Emma C. Kahle[2], Tyler R. Jones[9], Ayako Abe-Ouchi[4], Takashi Obase[4], Carlos Martin[10], Hugh Corr[10], Jeffrey P. Severinghaus[11], Ross Beaudette[11], Jenna A. Epifanio[1], Edward J. Brook[1], Kaden Martin[1], Jérôme Chappellaz[5], Shuji Aoki[12], Takakiyo Nakazawa[12], Todd A. Sowers[13], Richard B. Alley[13], Jinho Ahn[14], Michael Sigl[15], Mirko Severi[16,17], Nelia W. Dunbar[18], Anders Svensson[19], John M. Fegyveresi[20], Chengfei He[21], Zhengyu Liu[21], Jiang Zhu[22], Bette L. Otto-Bliesner[22], Vladimir Y. Lipenkov[23], Masa Kageyama[24], Jakob Schwander[15]

Water-stable isotopes in polar ice cores are a widely used temperature proxy in paleoclimate reconstruction, yet calibration remains challenging in East Antarctica. Here, we reconstruct the magnitude and spatial pattern of Last Glacial Maximum surface cooling in Antarctica using borehole thermometry and firn properties in seven ice cores. West Antarctic sites cooled ~10°C relative to the preindustrial period. East Antarctic sites show a range from ~4° to ~7°C cooling, which is consistent with the results of global climate models when the effects of topographic changes indicated with ice core air-content data are included, but less than those indicated with the use of water-stable isotopes calibrated against modern spatial gradients. An altered Antarctic temperature inversion during the glacial reconciles our estimates with water-isotope observations.

Using oxygen and hydrogen isotope ratios in ancient polar ice as records of past site temperature requires a calibration (*1*). Surface temperature and the isotopic composition of precipitation correlate spatially in Antarctica, with a regression coefficient α_S (spatial slope) of 0.80 per mil per kelvin (‰K^{-1}) for $\delta^{18}O$ (the ratio of ^{18}O to ^{16}O) (*2*). Reconstructing past temperatures requires regression over time, and this temporal slope α_T may differ from α_S. In East Antarctica, where the longest continuous ice core records, going back to 800 thousand years before present (ka BP), have been extracted (*3*), independent temperature estimates are not available, and the spatial slope is commonly used to convert isotopic ratios to temperature (*1*); this approach gives a surface temperature difference ΔT_S of around −9°C between the Last Glacial Maximum (LGM) (26 to 18 ka BP) and the preindustrial period (*1*, *4*, *5*).

Antarctic LGM-preindustrial isotope changes depend on many factors, including hemispheric sea surface temperatures (*6*), sea ice extent (*7*), ice sheet elevation (*8*), vapor origin and transport, precipitation seasonality, and post-depositional isotopic exchange (*9*). Isotope-enabled general circulation models seek to capture these physical processes, making them an invaluable tool for studying isotopic variations. Such models simulate LGM-preindustrial α_T ranging from 0.3 to 1.4 ‰K^{-1} in central East Antarctica (implied ΔT_S of −4° to −20°C), which implies that several aforementioned processes are poorly constrained (*8*, *10*–*12*).

We distinguish three temperatures: (i) the climatic temperature T_{CLIM} at constant elevation (relative to the present-day geoid); (ii) the surface temperature T_S, which may differ from the climatic temperature because of changing ice sheet topography; and (iii) the vapor condensation temperature T_C, which is warmer than the surface because of the strong Antarctic inversion (*2*, *13*).

In this study, we empirically reconstruct LGM surface temperature across Antarctica (Fig. 1) using two independent methods. We investigated five East Antarctic ice cores—EPICA (European Project for Ice Coring in Antarctica) Dome C (EDC), EPICA Dronning Maud Land (EDML), Dome Fuji (DF), Talos Dome (TAL), and South Pole (SP)—and two West Antarctic cores—West Antarctic Ice Sheet (WAIS) Divide (WD) and Siple Dome (SDM).

First, we estimated ΔT_S at EDC and DF from the measured borehole temperature profiles (Fig. 2) using a method similar to that used recently at WD (*14*). Owing to the downward ice flow and low thermal diffusivity, the ice sheet maintains an imprint of its past surface temperature history. The large ice sheet thickness at EDC and DF is favorable for preserving past temperatures, yet the low accumulation rate is not. Consequently, the relative uncertainty in the EDC and DF borehole reconstructions is larger than that at WD. To constrain the problem better, we used downward ice velocities measured by means of phase-sensitive radio-echo sounding (EDC only) and accurate age constraints derived through volcanic synchronization to the layer-counted WD time scale.

We forced a one-dimensional heat transport–ice flow model at the surface boundary with a temperature history that is based on the $\delta^{18}O$ record scaled with a constant α_T value (*10*). Applying traditional isotope scaling ($\alpha_T \approx$ 0.7 ‰K^{-1}, yielding ΔT_S = −9°C at EDC and −7.5°C at DF) simulates temperature profiles that do not fit the borehole observations at either site (Fig. 2). At EDC, the model-data fit is optimized for α_T = 1.14 ‰K^{-1}, which is consistent with ΔT_S = −5.5°C (95% confidence range is −6.9° to −3.1°C). At DF, the optimal ΔT_S is in the −2.0° to −5.4°C range; we provide a range without a best estimate because, at DF, there are no direct constraints on the downward ice velocity. In Fig. 1, the WD, EDC, and DF borehole estimates are marked "BH."

Second, we reconstructed past climate at all seven sites using the dependence of firn densification, the gradual transformation of polar snow to ice, on T_S and accumulation rate (*A*). Air bubbles are isolated from the atmosphere at the lock-in depth (50 to 120 m below the surface), an event preserved in two ice core signals (*15*): $\delta^{15}N$ of N_2 which records past firn column thickness by means of gravitational enrichment, and the gas age–ice age difference, or Δage. The $\delta^{15}N$ and Δage-isopleths are perpendicular in T_S-*A* space (Fig. 3A), meaning that if $\delta^{15}N$ and Δage are independently known, a distinctive climatic (T_S, *A*)

[1]College of Earth Ocean and Atmospheric Sciences, Oregon State University, Corvallis, OR 97331, USA. [2]Department of Earth and Space Science, University of Washington, Seattle, WA 98195, USA. [3]Geographical and Environmental Sciences, Northumbria University, Newcastle, UK. [4]Atmosphere and Ocean Research Institute, The University of Tokyo, Kashiwa 277-8568, Japan. [5]Université Grenoble Alpes, CNRS, IRD, IGE, Grenoble, France. [6]National Institute of Polar Research, Tachikawa, Tokyo, Japan. [7]Department of Polar Science, The Graduate University of Advanced Studies (SOKENDAI), Tokyo, Japan. [8]Japan Agency for Marine Science and Technology (JAMSTEC), Yokosuka, Japan. [9]Institute of Arctic and Alpine Research, University of Colorado, Boulder, CO 80309, USA. [10]British Antarctic Survey, Cambridge, UK. [11]Scripps Institution of Oceanography, University of California, San Diego, La Jolla, CA 92093, USA. [12]Center for Atmospheric and Oceanic Studies, Graduate School of Science, Tohoku University, Sendai 980-8578, Japan. [13]The Earth and Environmental Systems Institute, Pennsylvania State University, University Park, PA 16802, USA. [14]School of Earth and Environmental Sciences, Seoul National University, Seoul 08826, South Korea. [15]Climate and Environmental Physics, Physics Institute & Oeschger Center for Climate Change Research, University of Bern, 3012 Bern, Switzerland. [16]Department of Chemistry "Ugo Schiff," University of Florence, Florence, Italy. [17]Institute of Polar Sciences, ISP-CNR, Venice-Mestre, Italy. [18]New Mexico Bureau of Geology & Mineral Resources, Earth and Environmental Science Department, New Mexico Tech, Socorro, NM 87801, USA. [19]Niels Bohr Institute, University of Copenhagen, Copenhagen, Denmark. [20]School of Earth and Sustainability, Northern Arizona University, Flagstaff, AZ 86011, USA. [21]Department of Geography, Ohio State University, Columbus, OH 43210, USA. [22]National Center for Atmospheric Research, Boulder, CO 80307, USA. [23]Climate and Environmental Research Laboratory, Arctic and Antarctic Research Institute, St. Petersburg 199397, Russia. [24]Laboratoire des Sciences du Climat et de l'Environnement-IPSL, Université Paris-Saclay, Gif-sur-Yvette, France.
***Corresponding author. Email: christo.buizert@oregonstate.edu**

solution exists (subject to the uncertainties of the firn model).

Synchronization using both volcanic deposits and globally synchronous abrupt atmospheric methane variations allowed us to estimate Δage empirically for the Antarctic ice cores (*10*, *16*). We used an inverse dynamical firn densification–heat transport model (*17*, *18*) to reconstruct T_S and A histories that optimize the fit to Δage and δ^{15}N data (Fig. 3, B and C). Reconstructed accumulation rates agree (within uncertainty) with independent estimates (fig. S8). Methodological biases and uncertainties are estimated by using a Monte Carlo approach (*10*). The histograms in Fig. 1 give the ΔT_S distribution of the Δage-based reconstruction.

In East Antarctica, ΔT_S ranges from −3.8° ± 2.0°C (DF) to −7.1° ± 1.7°C (TAL); at DF, EDC, and EDML, ΔT_S is substantially lower than estimates from isotope scaling that use α_S. The two West Antarctic sites have similar ΔT_S of −10.2° ± 2.4°C (SDM) to −10.3° ± 1.3°C (WD). The Δage- and borehole-based reconstruction methods agree within uncertainty at all sites (Fig. 1). Allowing for more flank-like ice flow at EDC during the glacial period (which would occur if the divide position were different from that at present) improves the agreement by changing the borehole estimate to around −4.5°C (*10*); we choose to report the −5.5°C value to keep both methods independent. PMIP4 (Paleoclimate Modeling Intercomparison Project phase 4) simulations (*19*) find a seven-site-mean ΔT_S magnitude that is 1.2° ± 4.6°C larger than our Δage-based reconstructions (mean and spread of 10 climate models; Fig. 1).

We emphasize that the firn method is primarily constrained by the empirical Δage estimates. Because T_S and A broadly covary via the saturation vapor pressure, the deglacial climatic changes run parallel to the δ^{15}N-isopleths (Fig. 3A). Therefore, δ^{15}N data alone do not constrain the magnitude of climate change meaningfully. The effects of T_S and A are additive in Δage, however, making Δage a sensitive proxy for climate change (Fig. 3D), as first noted by Schwander *et al.* (*20*). The empirical Δage at 24 ka BP is larger than at 18 ka BP for all five cores where both are available, and coldest conditions in Antarctica occur ~27 to ~24 ka BP in our reconstructions (fig. S8h); this follows expectations from local insolation (*21*).

We propose that elevation changes explain the spatial differences in ΔT_S (*8*). Let Δz be the LGM elevation anomaly relative to the present. We present WD and DF total air-content data (fig. S12) and interpret them in terms of elevation change (*22*). These data suggest a 420-m (range, 280 to 590 m) contrast in Δz between WD and central East Antarctica (here, DF and EDC)—for example, Δz = +300 m at WAIS and Δz = −120 m in central East Antarctica (Fig. 4B). Our estimate is broadly in agreement with LGM ice sheet reconstructions that suggest a West-East Δz contrast between 160 and 560 m (*10*). Although the implied Δz at WAIS exceeds the observed highstand at ice margin nunataks (*23*), such data do not strongly constrain the elevation at WD more than 500 km away. The corresponding ΔT_S contrast (WD ΔT_S minus the average ΔT_S at DF and EDC) is −6.2° ± 2.3°C in the Δage-based reconstructions, −6.0° ± 2.0°C in the borehole reconstructions, and −5.9° ± 2.7°C in the PMIP4 model ensemble; the level of agreement suggests this is a robust feature of Antarctic LGM climate. This temperature contrast is thus plausibly linked to Δz through the (spatial) lapse rate in the interior of Antarctica of around −12°C km^{-1} (*2*, *24*).

To further assess the elevation impact on ΔT_S, we perform an atmosphere-ocean general circulation model (AOGCM) sensitivity study of Antarctic LGM climate using the MIROC (Model for Interdisciplinary Research on Climate) and HadCM3 (Hadley Centre Coupled Model version 3) models and a series of LGM topographic reconstructions (*10*). We first estimated climatic LGM cooling using full LGM boundary conditions (including LGM albedo) but preindustrial Antarctic topography; this yielded a seven-site average ΔT_{CLIM} of −4.7° and −7.0°C in the MIROC and HadCM3 models, respectively, but stronger albedo-driven cooling is found over the Ross and Weddell Seas due to ice growth onto the continental shelf (Fig. 4A). Simulated climatic ΔT_{CLIM} is similar in interior West and East Antarctica in the absence of topographic change.

Next, we performed climate simulations with five Antarctic LGM topographic reconstructions. These reconstructions suggest Δz of +100 to +600 m in interior WAIS and down to −250 m in interior East Antarctica (Fig. 4B). These changes result in greater ΔT_S in West than in central East Antarctica (Fig. 4C), in agreement with our reconstructions. By comparing the various topographic reconstructions, we find that ΔT_S is closely linked to Δz in both models through the dry adiabatic lapse rate of −9.8°C km^{-1} (Fig. 4D). Also, a fraction of the variance is due to the topography altering the atmospheric circulation around Antarctica, rather than the direct lapse-rate effect. We find a correlation r = 0.96 between the reconstructed and the simulated site ΔT_S pattern (averaged across the five topographic reconstructions and both models); for the PMIP4 multimodel mean, this correlation is r = 0.95. We conclude that changes in LGM ice sheet topography plausibly explain the ΔT_S spatial variability in our reconstruction (*8*).

Our findings have implications for the interpretation of water isotopes in Antarctic ice cores. We found α_T in the range of 0.9 to 1.4 ‰K^{-1} in East Antarctica and, therefore, $\alpha_T > \alpha_S$, opposite to Greenland, where $\alpha_T < \alpha_S$ (*17*, *25*). We compared our α_T with those from LGM and preindustrial simulations using the latest-generation isotope-enabled Community Earth System Model (iCESM) (Fig. 4E). The

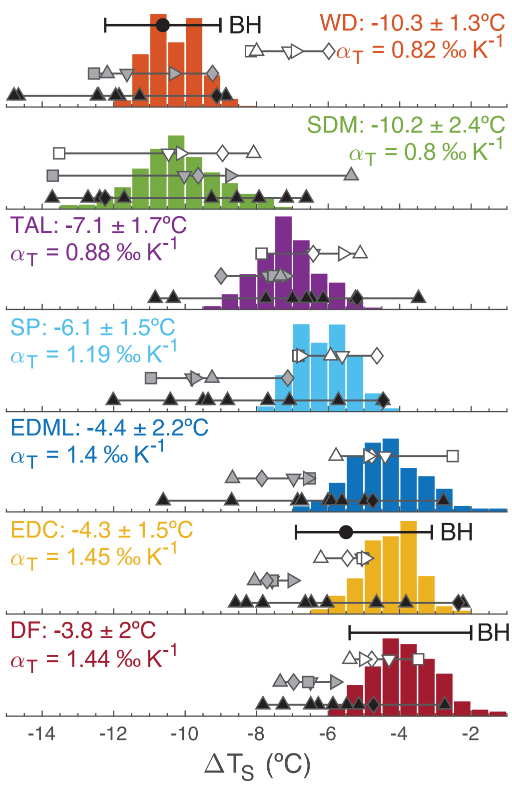

Fig. 1. Summary of Antarctic LGM cooling estimates. Black markers with horizontal error bars marked "BH" give borehole estimates; WD results are from (*14*). Histograms give distribution of Δage-based temperature reconstructions from a Monte Carlo sampling (N = 1000) of model parameters; listed are mean and 2σ standard deviation of the distribution, as well as the implied temporal isotope slope α_T. ΔT_S is the LGM (18 to 21.4 ka BP) minus preindustrial (0.5 to 2.5 ka BP) condition. White (MIROC), gray (HadCM3), and black (PMIP4) show AOGCM-simulated ΔT_S, with symbols denoting different LGM topography reconstructions (*10*): Pollard and Deconto (downward triangle) (*32*); Whitehouse *et al.* (square) (*33*); Glac-1D (diamond) (*29*); Golledge *et al.* (rightward triangle) (*34*); and Ice-6G (upward triangle).

good agreement (r = 0.91; 0.06 ‰K^{-1} mean offset) demonstrates that our reconstructed α_T are consistent with isotope physics, yet the large intermodel spread in simulated α_T [see section S3.5 in (*10*) for a review] prevents us from claiming that it validates our results. Although the α_T agree well, iCESM simulated a ΔT_S and LGM-preindustrial $\delta^{18}O$ change that are both too large (compared with our reconstructions and ice core data, respectively).

Last, we investigated changes to the strong surface-based inversion in the Antarctic boundary layer (Fig. 4F). The condensation temperature T_C is higher than T_S, and they correlate spatially with a slope dT_C/dT_S in the 0.63 to 0.67 range (*2*, *13*, *26*). T_C controls precipitation $\delta^{18}O$, with a present-day spatial sensitivity of $d\delta^{18}O/dT_C = d\delta^{18}O/dT_S \times dT_S/dT_C \approx 0.80/0.65 = 1.23$ ‰K^{-1}. We now assume that, unlike ΔT_S, the LGM-preindustrial change ΔT_C can be estimated by using this spatial slope via $\Delta T_C = \Delta\delta^{18}O/1.23$ (Fig. 4F). At WD and SDM, the $\alpha_T \approx \alpha_S$ assumption holds, suggesting that the ratio $\Delta T_C/\Delta T_S$ is close to the present-day ratio of 0.65; in central East Antarctica, the ratio $\Delta T_C/\Delta T_S$ exceeds 0.65, which is consistent with $\alpha_T > \alpha_S$. We plotted simulated ΔT_S versus ΔT_C across interior Antarctica from a wide range of AOGCMs and topographies; we found that the ratio $\Delta T_C/\Delta T_S$ ranges from 0.48 to 1.3 (95% interval, gray lines), with our empirical reconstructions falling within the model data cloud (Fig. 4F). In aggregate, these simulations find that $\Delta T_C/\Delta T_S$ tends to exceed the present-day ratio of 0.65 (~79% of model data points); such a change to the inversion structure would result in $\alpha_T > \alpha_S$ for ΔT_S. In the iCESM simulations, the $\Delta T_C/\Delta T_S$ and α_T fields look similar, with the $\Delta T_C/\Delta T_S = 0.65$ contour line broadly aligning with the α_T = 0.8 ‰K^{-1} contour line (fig. S11). We conclude that physically plausible changes to the inversion (*27*, *28*) may reconcile our reconstructions with previous work on Antarctic LGM water isotopes.

Our reconstructions improve the LGM Antarctic temperature estimation and provide a benchmark for testing the ability of (isotope-enabled) climate models to simulate climate states radically different from the late

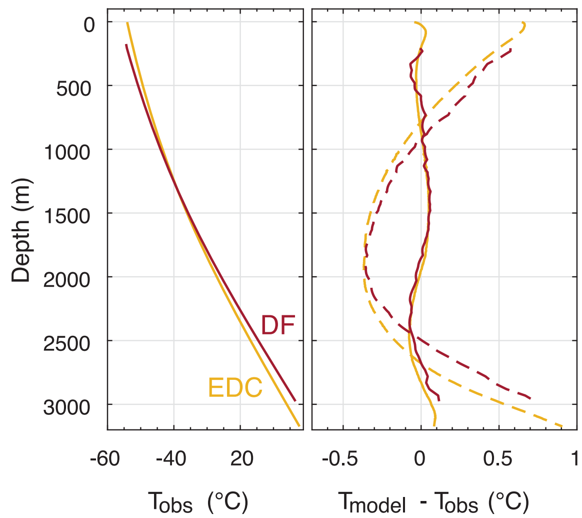

Fig. 2. Borehole temperature reconstruction for EDC and DF. (Left) Site borehole temperature observations at EDC (yellow) and DF (red). At both sites, the ice-bedrock interface is at the pressure melting point (−2.2°C). (Right) Model-data mismatch at EDC (yellow) and DF (red) for an ice flow–heat transport model forced by the optimized temperature histories (solid lines, ΔT_S of −5.5°C at EDC and −3.2°C at DF) and forced with water-isotope scaling of 0.7 ‰K^{-1} (dashed lines, ΔT_S of −9.0°C at EDC and −7.5°C at DF).

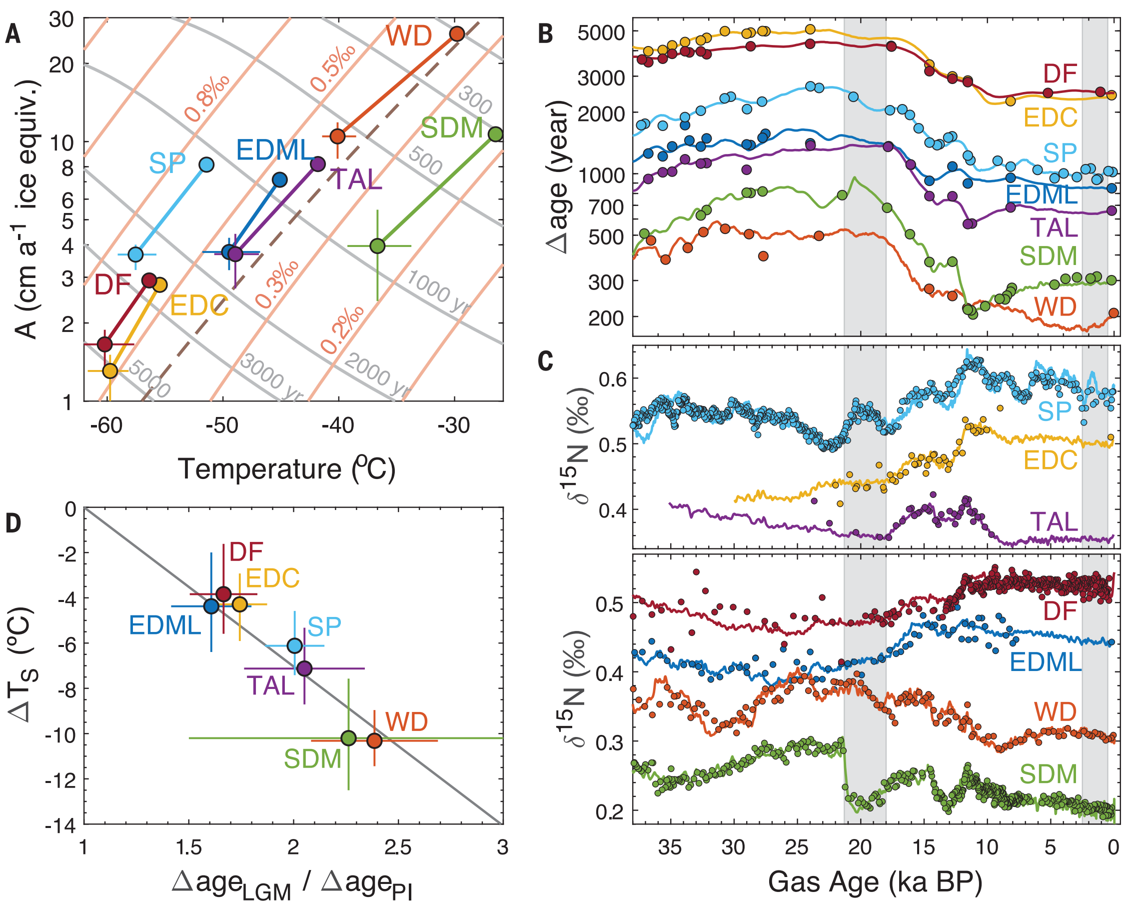

Fig. 3. Δage-based temperature reconstructions. (**A**) Δage and $\delta^{15}N$-isopleths (gray and salmon, respectively) in the steady-state Herron-Langway firn densification model as a function of T_S and A. The dashed line shows accumulation scaling by means of the saturation vapor pressure at the site (ignoring the atmospheric inversion). Reconstructed preindustrial and LGM conditions at the seven sites are indicated. (**B**) Model fit to empirical Δage constraints. Gray vertical bars denote the LGM (21.4 to 18 ka BP) and preindustrial (2.5 to 0.5 ka BP) periods. (**C**) Model fit to $\delta^{15}N$ data, divided over two panels to prevent overlapping curves. Data are shown on the WD2014 time scale (*30*, *31*). (**D**) Reconstructed ΔT_S versus ratio of LGM Δage over preindustrial Δage (with linear fit) (Δage_{PI}), showing the utility of Δage as a climate proxy.

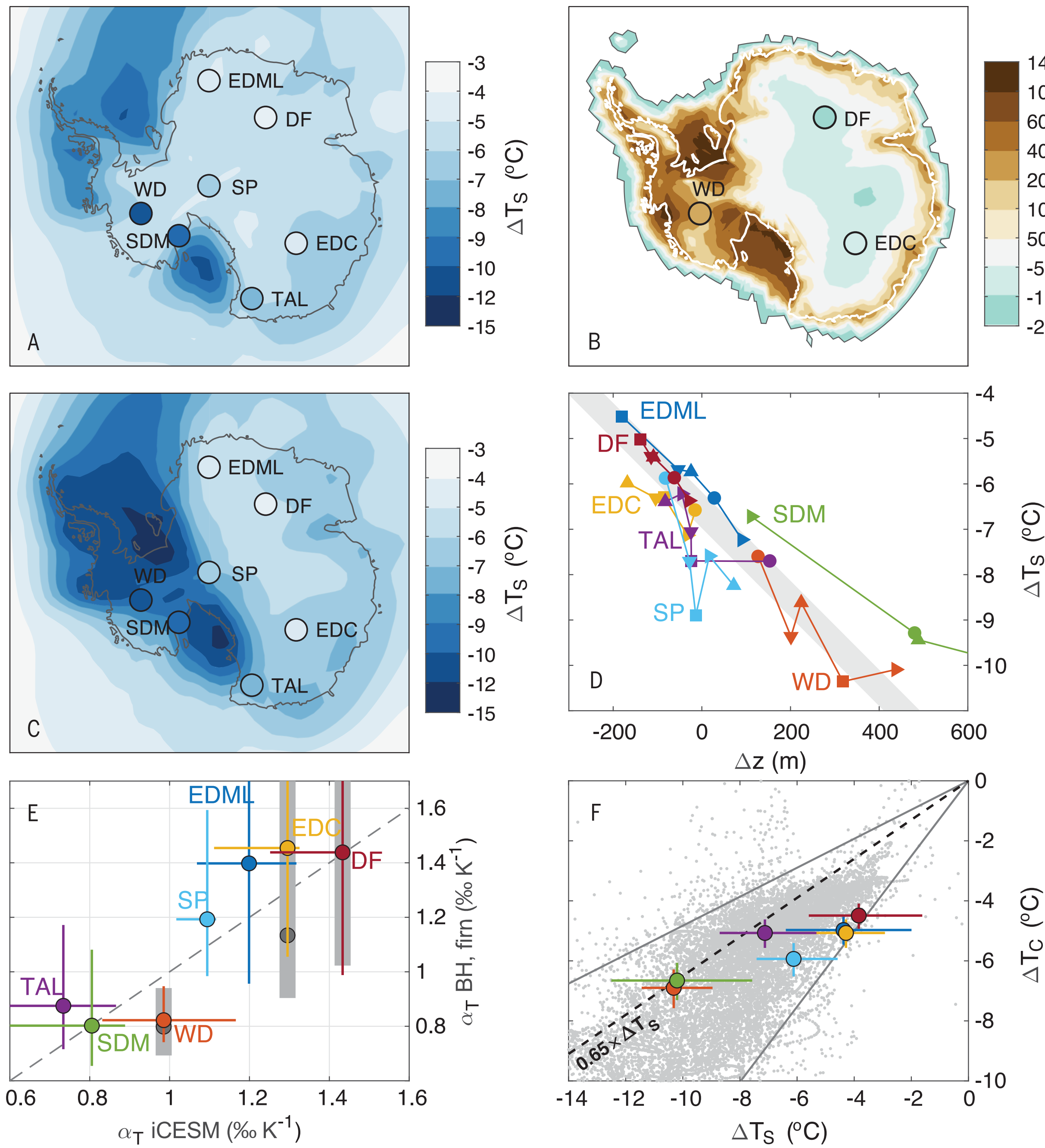

Fig. 4. Climate models and Antarctic topography. (**A**) AOGCM simulations of ΔT_S using preindustrial ice topography in Antarctica (average of MIROC and HadCM models), with Δage-based ΔT_S reconstructions for the seven sites. (**B**) Simulated LGM elevation anomaly (shaded, average of five topographies) with LGM elevation anomaly of +310, −80, and −140 m at WD, EDC, and DF (*10*). (**C**) As in (A), but using LGM ice topography in Antarctica (average of five LGM topographies and both MIROC and HadCM models). (**D**) Elevation change versus ΔT_S in the AOGCM simulations (average of MIROC and HadCM models); symbols denote the different LGM topographic reconstructions (see Fig. 1 caption for legend). The gray bar shows the dry adiabatic lapse rate. (**E**) Temporal isotope slope α_T from the iCESM model against our reconstructions (borehole in gray, Δage-based in colors). (**F**) ΔT_S versus ΔT_C from Δage-based ΔT_S and isotope-based ΔT_C (large dots with error bars) and from LGM-preindustrial AOGCM simulations (small gray dots, gray lines enclose the central 95% of estimates); the black dashed line represents the modern spatial slope (*2*). Models plotted are PMIP3 [except for one model that simulates ΔT_S > 0°C], PMIP4 (all model output publicly available), and all iCESM, MIROC, and HadCM3 simulations used in this work; we show interior Antarctica (surface pressure < 800 hPa); T_C is taken to be the annual mean troposphere temperature maximum (typically ~500 hPa). The models have an average preindustrial spatial dT_C/dT_S of 0.68 (range, 0.31 to 0.89) in interior Antarctica.

Holocene. For surface temperature, the spatial isotopic slope is not always a good approximation of the temporal slope, challenging the prevalent interpretation of ice core water isotopes in Antarctica.

REFERENCES AND NOTES

1. J. Jouzel *et al.*, *J. Geophys. Res.* **108**, 4361 (2003).
2. V. Masson-Delmotte *et al.*, *J. Clim.* **21**, 3359–3387 (2008).
3. L. Augustin *et al.*, *Nature* **429**, 623–628 (2004).
4. V. Masson-Delmotte *et al.*, *Quat. Sci. Rev.* **29**, 113–128 (2010).
5. J. Jouzel *et al.*, *Science* **317**, 793–796 (2007).
6. C. Risi, S. Bony, F. Vimeux, J. Jouzel, *J. Geophys. Res.* **115**, D12118 (2010).
7. D. Noone, I. Simmonds, *J. Geophys. Res.* **109**, D07105 (2004).
8. M. Werner, J. Jouzel, V. Masson-Delmotte, G. Lohmann, *Nat. Commun.* **9**, 3537 (2018).
9. M. Casado *et al.*, *Cryosphere* **12**, 1745–1766 (2018).

10. Materials and methods are available as supplementary materials.
11. J.-E. Lee, I. Fung, D. J. DePaolo, B. Otto-Bliesner, *J. Geophys. Res.* **113**, D19109 (2008).
12. G. Hoffmann, J. Jouzel, V. Masson, *Hydrol. Processes* **14**, 1385–1406 (2000).
13. J. Jouzel, L. Merlivat, *J. Geophys. Res.* **89**, 11749–11757 (1984).
14. K. M. Cuffey *et al*., *Proc. Natl. Acad. Sci. U.S.A.* **113**, 14249–14254 (2016).
15. T. Sowers, M. Bender, D. Raynaud, Y. S. Korotkevich, *J. Geophys. Res.* **97**, 15683–15697 (1992).
16. J. A. Epifanio *et al*., *Clim. Past* **16**, 2431–2444 (2020).
17. C. Buizert *et al*., *Science* **345**, 1177–1180 (2014).
18. M. M. Herron, C. C. Langway, *J. Glaciol.* **25**, 373–385 (1980).
19. M. Kageyama *et al*., *Geosci. Model Dev.* **10**, 4035–4055 (2017).
20. J. Schwander *et al*., *J. Geophys. Res.* **102**, 19483–19493 (1997).
21. P. Huybers, G. Denton, *Nat. Geosci.* **1**, 787–792 (2008).
22. D. Raynaud *et al*., *Earth Planet. Sci. Lett.* **261**, 337–349 (2007).
23. P. Spector, J. Stone, B. Goehring, *Cryosphere* **13**, 3061–3075 (2019).
24. J. Fortuin, J. Oerlemans, *Ann. Glaciol.* **14**, 78–84 (1990).
25. K. M. Cuffey *et al*., *Science* **270**, 455–458 (1995).
26. W. Connolley, *Int. J. Climatol.* **16**, 1333–1342 (1996).
27. G. Krinner, C. Genthon, *Clim. Dyn.* **14**, 741–758 (1998).
28. N. P. M. Van Lipzig, E. Van Meijgaard, J. Oerlemans, *J. Glaciol.* **48**, 611–621 (2002).
29. L. Tarasov, A. S. Dyke, R. M. Neal, W. R. Peltier, *Earth Planet. Sci. Lett.* **315–316**, 30–40 (2012).
30. C. Buizert *et al*., *Clim. Past* **11**, 153–173 (2015).
31. M. Sigl *et al*., *Clim. Past* **12**, 769–786 (2016).
32. D. Pollard, R. M. DeConto, *Nature* **458**, 329–332 (2009).
33. P. L. Whitehouse, M. J. Bentley, A. M. Le Brocq, *Quat. Sci. Rev.* **32**, 1–24 (2012).
34. N. R. Golledge *et al*., *Nat. Commun.* **5**, 5107 (2014).
35. Computational and Information Systems Lab, Cheyenne: HPE/SGI ICE XA System (University Community Computing) (National Center for Atmospheric Research, 2019); https://doi.org/10.5065/D6RX99HX.

ACKNOWLEDGMENTS

The idea of weak East Antarctic LGM cooling was suggested a decade ago by S. J. Johnsen (1940–2013) and J. Schwander but never published. We thank E. Capron and A. Landais for help in gathering δ^{15}N data; T. Hondoh and T. Kameda for support in Dome Fuji air-content analyses; C. Bréant for sharing model output; V. Gkinis for useful discussions; W.-L. Chan for assistance with model analysis; J.-Y. Peterschmitt for compiling PMIP4 model data and all PMIP4 groups for sharing model output; and C. Adams of Corvidopolis for providing a toddler-free work space during the COVID-19 pandemic. **Funding:** This work was supported by the US National Science Foundation (NSF) (grants 1643394 to C.B.; 1643355 to T.J.F. and E.J.S.; 1602435, 1443105, 1141839, 1043092, 0537930, and 1443105 to E.J.S.; 1443472 and 1643722 to E.J.B.; and 1738934 to R.B.A.); the University of Washington Royalty Research Fund (to T.J.F.); MEXT and the Japan Society for the Promotion of Science KAKENHI (grant numbers 18749002, 26241011, 15KK0027, 17H06316, and 20H00639 to K.K.; 20H04327 to I.O.; 22310003 to T.N.; and 15J12515, 17H06104, 17H06323, and 20K14552 to A.A.-O.); the National Research Foundation of Korea (NRF) (grants NRF-2018R1A2B3003256 and NRF-2018R1A5A1024958 to J.A.); the European Research Council (ERC) under the European Union's Horizon 2020 research and innovation program (grant agreement no. 820047 to M.Si.); IT-MIUR-PNRA (Italian Antarctic Research Program) through the BE-OI (PNRA16_00124) project (to M.Se.); the Villum Investigator Project IceFlow (NR. 16572 to A.S.); Beyond EPICA - Oldest Ice Core EU Coordination and Support Action; measurements at EDC (Concordia Station) were supported by the French Polar Institute (IPEV, prog. 902) and the Italian Antarctic Program (PNRA and ENEA). The Talos Dome Ice core Project (TALDICE), a joint European program, is funded by national contributions from Italy, France, Germany, Switzerland, and the United Kingdom. Primary logistical support was provided by PNRA at Talos Dome. This is TALDICE publication no 59. The CESM project is supported primarily by the NSF. This material is based upon work supported by the National Center for Atmospheric Research (NCAR), which is a major facility sponsored by the NSF under cooperative agreement no. 1852977 (B.L.O.-B.). Computing and data storage resources, including the Cheyenne supercomputer (*35*), were provided by the Computational and Information Systems Laboratory at NCAR (Z.L., C.H., and B.L.O.-B.). **Author contributions:** C.B., E.J.S., and W.H.G.R. conceived of the study; Δage-based reconstructions were by C.B.; ice flow and borehole temperature modeling were by T.J.F. and C.R.; GCM modeling was by W.H.G.R., S.S.-T., T.O., A.A.-O., C.H., Z.L., J.Z., and B.L.O.-B.; PMIP4 model compilation was by M.K.; methane data were by E.J.B., J.E., J.A., K.M., J.C., T.A.S., K.K., S.A., and T.N.; δ^{15}N-N_2 data were by I.O., K.K., R.B., J.P.S., S.A., and T.N.; borehole thermometry data were by C.R., E.L., and H.M.; ApRES data were by C.M. and H.C.; SP isotope data were by E.J.S., E.C.K., and T.R.J.; air-content data and corrections were by J.E., K.K., V.L., J.M.F., and R.B.A.; SDM chronology was by T.J.F. and C.B.; SDM tephra matches were by N.W.D.; volcanic matching was by M.Si., M.Se., A.S., T.J.F., and C.B.; J.S. independently performed a similar study that reached the same conclusion around a decade ago; all authors contributed toward the final manuscript. **Competing interests:** The authors declare no competing interests. **Data and materials availability:** All new ice core data from this study are available in the supplementary materials as Data S1 and online at www.ncdc.noaa.gov/paleo/study/32632; previously published data are available with their original publications and/or in publicly accessible online data archives. Climate model output is available at http://dods.lsce.ipsl.fr/pmip4/db/ or upon request from the corresponding author.

SUPPLEMENTARY MATERIALS

science.sciencemag.org/content/372/6546/1097/suppl/DC1
Materials and Methods
Figs. S1 to S12
Tables S1 to S7
References (*36–160*)
Data S1

18 June 2020; accepted 29 April 2021
10.1126/science.abd2897

Antarctic surface temperature and elevation during the Last Glacial Maximum

Christo Buizert, T. J. Fudge, William H. G. Roberts, Eric J. Steig, Sam Sherriff-Tadano, Catherine Ritz, Eric Lefebvre, Jon Edwards, Kenji Kawamura, Ikumi Oyabu, Hideaki Motoyama, Emma C. Kahle, Tyler R. Jones, Ayako Abe-Ouchi, Takashi Obase, Carlos Martin, Hugh Corr, Jeffrey P. Severinghaus, Ross Beaudette, Jenna A. Epifanio, Edward J. Brook, Kaden Martin, Jrme Chappellaz, Shuji Aoki, Takakiyo Nakazawa, Todd A. Sowers, Richard B. Alley, Jinho Ahn, Michael Sigl, Mirko Severi, Nelia W. Dunbar, Anders Svensson, John M. Fegyveresi, Chengfei He, Zhengyu Liu, Jiang Zhu, Bette L. Otto-Bliesner, Vladimir Y. Lipenkov, Masa Kageyama, and Jakob Schwander

Science, **372** (6546), .
DOI: 10.1126/science.abd2897

Antarctic paleotemperatures
It has been widely thought that East Antarctica was #9°C cooler during the Last Glacial Maximum, close to the #10°C difference between then and now determined independently for West Antarctica. Buizert *et al.* used borehole thermometry, firn density reconstructions, and climate modeling to show that the temperature in East Antarctica was actually only #4° to 7°C cooler during the Last Glacial Maximum. This result has important consequences for our understanding of Antarctic climate, polar amplification, and global climate change.

Science, abd2897, this issue p. 1097